The role of hydrogen in copper

Rolf Sandström

Memo 2014-01-27 containing documentation to be used in the response to issues brought up by SSM

Summary

Recent research on hydrogen charging of copper is presented with focus on work carried out at Swerea KIMAB. With electrochemical charging the hydrogen content can be raised. It has been found that the hydrogen is localised to a thin surface layer with a thickness of about 50 μm. In this surface layer, hydrogen bubbles are formed. Since the mechanical damage is restricted to this thin surface layer, the mechanical integrity of the canister is not affected. A model has been developed that can explain and quantify the distribution of hydrogen and bubbles. The model can also describe the degassing of hydrogen, once the hydrogen charging has been stopped.

1. Effect of hydrogen on copper material

1.1. Hydrogen gas in canisters

Spent nuclear fuel is planned to be disposed of by encapsulation in cast iron inserts placed within copper shells. The role of the cast iron is to be load bearing, and the copper shell gives protection against corrosion from the outside. During the encapsulation process, there is a risk that some water is left inside the cast iron insert when the canister is sealed. According to the present design rules, a maximum of 600 g of water can be trapped inside the canister during manufacture (SKB 2006). Furthermore, inside the insert, radiolysis of water due to gamma radiation will generate hydrogen during an initial phase. Hydrogen is also formed due to corrosion of iron if there is a hole in the copper shell and groundwater is intruding. Most hydrogen released will eventually diffuse into the iron and possibly also into the copper. For this reason the build-up of hydrogen in copper is being studied.

1.2. Hydrogen embrittlement

Hydrogen embrittlement is a well-known phenomenon. Examples of hydrogen induced damage include formation of internal voids and cracks, loss of ductility, and high temperature hydrogen attack. Tensile stresses and the presence of hydrogen is necessary to cause classical hydrogen embrittlement.

Hydrogen embrittlement is an important issue in many application fields such as nuclear, chemical, petrochemical and marine industries. Examples of structures that may be affected include storage tanks, reaction vessels, pipelines, and compressors. The presence of hydrogen in the material can strongly impair mechanical properties (Au 2007, Louthan et al. 1972). Applications that involve high hydrogen concentrations such as hydride storage devices, high-pressure hydrogen systems, sour gas wells, and coal gasification plants are especially exposed.

Many mechanisms have been proposed for hydrogen embrittlement. In a number of materials the introduction of hydrogen can induce brittle failure. Without hydrogen the fracture is ductile with significant macroscopic plastic deformation. This has two main effects. In the presence of hydrogen the toughness and the formability (ductility) is much reduced which increases the risk for component failure. The microscopic nature of the failure can also change from transgranular where the failure goes through the grains to intergranular, where the failure takes place at the grain boundaries. This is usually associated with a reduction in toughness.

PDF rendering: DokumentID 1420051, Version 1.0, Status Godkänt, Sekretessklass Öppen

A number of excellent review papers exists on hydrogen embrittlement in metals, for example Cotterill (1961), Louthan (2008), Louthan et al. (1972), Lynch (2012) and Song and Curtin (2011). For the definition of the different mechanisms we will follow Lynch (2012). Hydrogen embrittlement (HE) can appear in a number of different ways. For "*Internal hydrogen embrittlement*" (IHE) hydrogen concentrations are present in areas with high hydrostatic stress that gives cracking at stresses well below the yield strength. On the other hand "*Hydrogen environment embrittlement*" (HEE) appears as subcritical cracking under sustained loads in hydrogen or hydrogen-sulphide gases. If hydrides are present, fracture of brittle hydrides can take place at and ahead of cracks. This is termed "hydride embrittlement".

Other types of hydrogen damage are "blistering" and "hydrogen attack". Blistering is a result of atomic hydrogen in solution that recombines to form high pressure hydrogen gas at inclusions, grain boundaries and other interfaces near the surface. Due to the high pressure, voids expand by plastic deformation causing swelling at the surface. *Hydrogen attack*, also called "*hydrogen reaction embrittlement*" (HRE), is found when materials such as steels and copper are exposed to hydrogen at elevated temperatures, giving hydrogen diffusion and reaction with carbides and oxides. As a result high-pressure methane and steam, respectively are created resulting in internal voids and cracks.

In high strength steels and superalloys, H in solid solution often embrittles the material by initiating a transition from ductile fracture (i.e. microvoid coalescence) to brittle intergranular fracture. This transition is followed by a dramatic loss in toughness and ductility. The main competing mechanisms for HE are *hydrogen-enhanced decohesion* (HEDE), *hydrogen-enhanced local plasticity* (HELP), and hydride formation and cleavage. According to the HEDE mechanism, the H atoms are considered to lower the surface energy of atomic planes and grain boundaries, which stimulates cleavage-like failure (Song and Curtin 2011). In the HELP mechanism, H is assumed to be concentrated in Cottrell atmospheres around dislocation cores. It has been demonstrated experimentally that the motion of dislocations can be significantly increased and the yield strength reduced. This gives rise to exhaustion of the strain capacity of the material and early failure (Song and Curtin 2011).

High-strength martensitic steels with yield strengths greater than about 1400 MPa are quite susceptible to IHE. A solute hydrogen concentration of only 0.5–1 ppm (wt.) is required to initiate cracking. For ferritic steels with strengths below 750 MPa higher concentrations ($\geq$10 ppm) are needed to cause cracking. Titanium alloys with α-β microstructures are susceptible to IHE for concentrations above 100 ppm. Nickel, aluminium alloys, austenitic steels (that do not form martensite during deformation) and copper alloys exhibit little (if any) susceptibility to IHE or HEE, and industrial problems in these materials are rare (Lynch 2012). For copper alloys no cases have been found in the literature. Thus, hydrogen does not give rise to propagating cracks in copper alloys. However, hydrogen can still influence the mechanical properties of copper alloys and the same behaviour is also observed for nickel, see section 1.3.

1.3. Influence on mechanical properties of copper

Studies of the effect of hydrogen on mechanical properties of copper are quite limited. In one study, Nieh and Nix (1980) first introduced oxygen in pure copper by heat treating at 800 ºC. After that the copper was heat treated in hydrogen at 600 ºC. They reported that after creep testing, creep cavities were formed at the oxides in the grain boundaries, which gave low creep strength and ductility.

This is an example of a classical form of hydrogen reaction embrittlement of copper. Earlier this was referred to as hydrogen sickness (Butomo et al. 1968). It is attributed to the creation of voids due to the reaction between diffusing hydrogen and cuprous oxide inclusions forming

PDF rendering: DokumentID 1420051, Version 1.0, Status Godkänt, Sekretessklass Öppen

water vapour (Caskey et al. 1976). Oxygen has a very low solubility in copper, and it forms interdendritic and grain boundary Cu_2O already during the metallurgical processing of the copper. In many applications the oxygen is of little importance. However, when the temperature is raised above approximately 400 °C, for instance during welding or heat treatment, hydrogen can react with the internally dispersed Cu_2O to form steam (Caskey et al. 1976). The large water molecules generated in the reaction do not diffuse easily in copper and form voids, particularly at grain boundaries, which makes the copper brittle.

To avoid hydrogen reaction embrittlement, oxygen free copper with and without phosphorus is used, Cu-OF and Cu-OFP. Phosphorus combines with oxygen to form P_2O_5 and phosphates in particular at higher oxygen content, which further reduces the amount of oxygen available for steam formation (Magnusson and Frisk 2013b). It has now been demonstrated industrially for many years that the application of oxygen free copper eliminates hydrogen reaction embrittlement.

Even in the absence of oxygen, hydrogen can influence the mechanical properties of copper. Hydrogen absorption has proven to have an effect on the mechanical properties in thin foils or sheets. In Al-Marahleh and El-Amoush (2005), Kim and Byrne (1985) and Panagopoulos and Zacharopoulos (1994) it was shown that the hardness is raised by hydrogen charging. In addition, it was demonstrated that the tensile strength and elongation could be modestly reduced (Panagopoulos and Zacharopoulos 1994). Nakahara (1988) and Okinaka and Straschil (1986) found that trapped hydrogen in copper deposits reduced the ductility. It should be pointed out that the investigations (Nakahara 1988, Okinaka and Straschil 1986) were performed on electroless copper deposits, which are porous and difficult to compare to the behaviour of bulk copper.

2. Hydrogen charging of copper

2.1. Charging tests

From the discussion in section 1.3, it is evident that very limited information on the influence of hydrogen on properties of copper are available in the literature. Although some changes in mechanical properties were observed, they were recorded on thin sheet and foils. In addition, in none of the cited references, any measurement of the hydrogen content had been made. Consequently, there is no way to correlate the amount of absorbed hydrogen to the observed changes in mechanical properties. For these reasons, SKB decided to start charging tests at Swerea-KIMAB.

Charging methods for copper and optimisation of electrochemical charging parameters have been investigated in several publications. Nakahara and Okinaka (1988) listed three different charging methods: thermal charging, electrochemical charging and hydrogen entrapment during electroless copper deposition, and listed their advantages and drawbacks. Later Nakahara and Okinaka (1989) analysed how additions of arsenic to the electrolyte used in electrochemical charging could improve the absorption of hydrogen. Arsenic reduces the recombination rate to hydrogen molecules that diffuse very slowly in copper. This has now become the standard procedure.

2.2. Thermal charging

The first attempts at KIMAB were made with thermal charging. Wampler et al. (1976) demonstrated that if copper was placed in high pressure hydrogen (80 atm) at high temperature (900 ºC), a hydrogen content of 7 wt.ppm could be reached. Unfortunately, there are several drawbacks with such an approach. Facilities for heat treatment in high pressure hydrogen are not readily available. In addition, it was shown that using higher temperatures than 700 ºC would result in grain growth, which would destroy the microstructure of the

PDF rendering: DokumentID 1420051, Version 1.0, Status Godkänt, Sekretessklass Öppen

copper and make any attempt to study the influence on mechanical properties meaningless (Martinsson et al. 2013). As a result thermal charging was performed at 600 and 675 ºC in 1 atm hydrogen. At 600 ºC the hydrogen content was significantly reduced, at 675 ºC the content was essentially unchanged in relation to the start condition where the content was 0.7 wt.ppm (Martinsson et al. 2013). It was concluded that thermal charging in 1 atm hydrogen could not reach increased hydrogen contents without the risk of dramatically modifying the microstructure.

2.3. Electrochemical charging

To introduce the hydrogen, cathodic charging was applied using a constant current (Martinsson and Sandström 2012). The negative pole on a power supply was connected by a copper wire twirled around the specimen or soldered to the end of the cylinders. H_2SO_4 was used in the electrolyte since it gives a higher driving force for hydrogen formation than Na_2SO_4. The conditions were selected to obtain maximum charging. Specimens were charged at room temperature for up to three weeks. The solubility of hydrogen in copper is very low. The level of the solubility has been analysed by Magnusson and Frisk (2013b). As a consequence, hydrogen bubbles were formed during charging, Fig. 1. The number of bubbles and their size decreases rapidly with increasing distance from the charged surface. In the past it has also been observed that hydrogen-charging of pure copper can nucleate and grow bubbles (Caskey et al. 1975, Condon and Schober 1993, Nakahara 1988, Wampler et al. 1976) Condon and Schober's literature review (Condon and Schober 1993) presents different mechanisms for bubble growth.

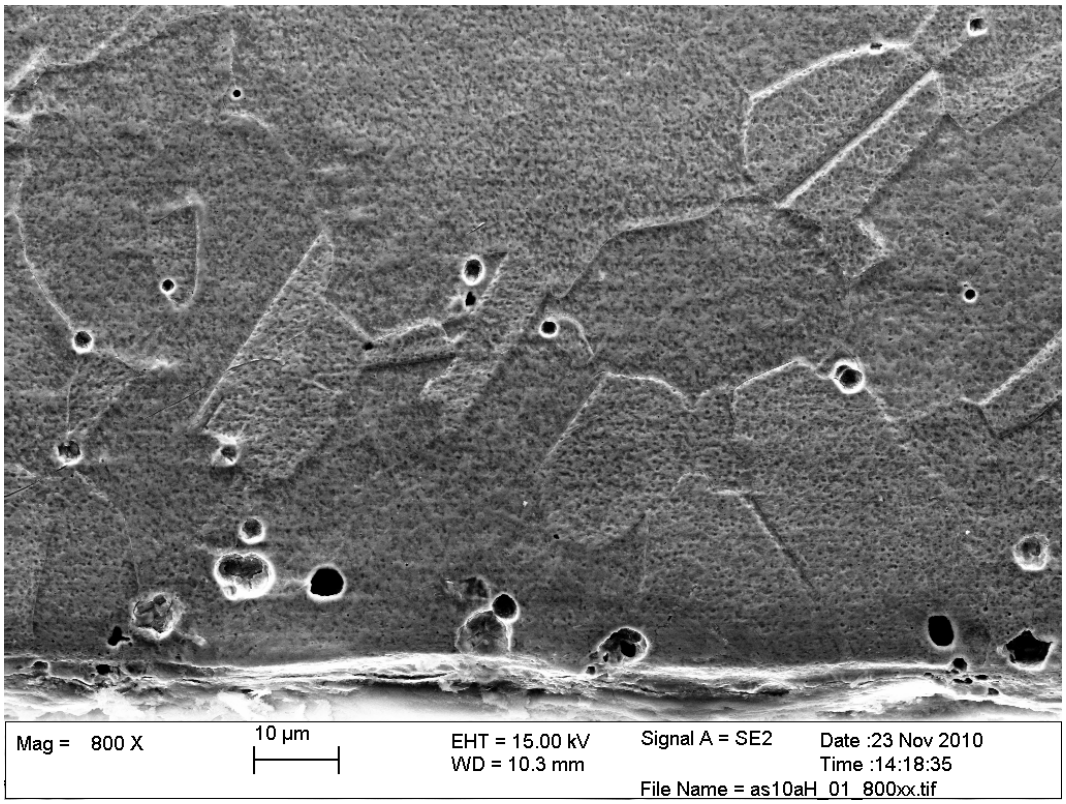

Fig. 1 Cross-section of a specimen hydrogen-charged for 3 weeks. The charged surface is at the bottom of the picture. Most hydrogen bubbles formed during charging are situated within 50 µm from the surface and are close to grain boundaries (Martinsson and Sandström 2012)

PDF rendering: DokumentID 1420051, Version 1.0, Status Godkänt, Sekretessklass Öppen

Glow Discharge Optical Emission Spectroscopy (GDOES) was used to measure the hydrogen content as a function of distance from the surface after charging. From the shape of the bubbles and with the help of elasto-plastic finite element analysis, it could be concluded that the hydrogen pressure in the bubbles was about 400 MPa (Martinsson and Sandström 2012). The size distribution of the bubbles was measured metallographically. Combining this information with the hydrogen pressure in the bubbles, an independent way of determining the amount hydrogen was obtained. The result is illustrated in Fig. 2. Each circle in the diagram is the average value of about 20 hydrogen bubbles. As can be seen, the amount of hydrogen decreases very rapidly with increasing distance from the surface. At a depth of 50 μm, the amount of hydrogen is two orders of magnitude lower than at the surface. At this depth, the hydrogen concentration is also close to the bulk value of the copper 0.6 wt.ppm before charging. It can be concluded that the charged hydrogen does not reach much more than 50 μm into the material. Fig. 2 also demonstrates that most of the hydrogen is present in the bubbles.

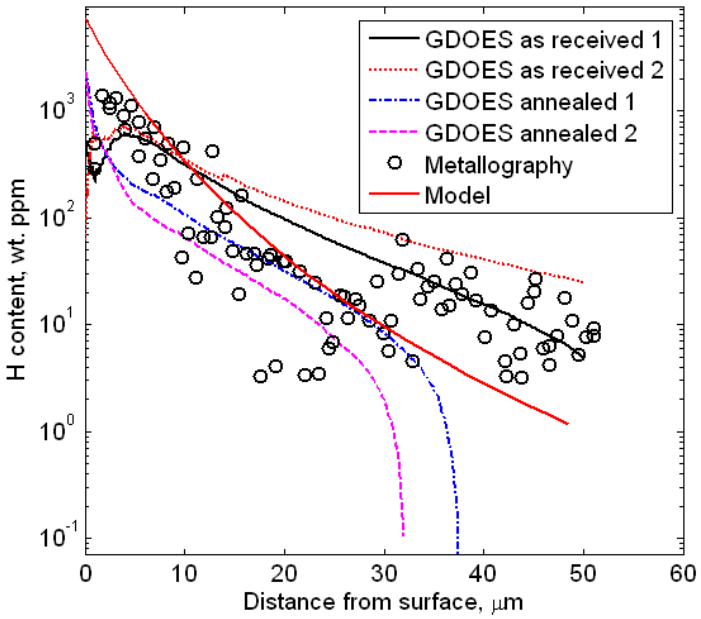

Fig. 2. Total hydrogen content versus distance from the surface after three weeks of charging. Model values are compared to the metallographic observations and GDOES data for four specimens (Martinsson and Sandström 2012).

2.4. Simultaneous charging and mechanical loading

A Finnish group has performed mechanical tests with simultaneous electrochemical charging (Yagodzinskyy et al. 2012). Two types of tests were carried out: slow strain rate tests at 20 and 50 ºC and simplified creep tests at constant load at 50 ºC. In the slow strain rate test a 10% reduction in tensile strength and elongation was observed at 50 ºC for the specimen that was charged. In the creep tests, an increase in the creep rate by up to a factor of three was found for charged specimens. In the tests at 50 ºC, a crack depth of about 100 μm was noted on the surfaces of charged specimens.

An analysis of the results from Yagodzinskyy et al. (2012) shows that the reduction in tensile strength could be explained. If it is assumed that half of the observed crack depth gives a reduction in load carrying area and considering the used specimen thickness of 1.3 mm, the relative loss in strength is 9%, very close to the value found. The measured stress strain

PDF rendering: DokumentID 1420051, Version 1.0, Status Godkänt, Sekretessklass Öppen

curves have a lower work hardening (lower slope) for hydrogen charged copper. It is well established that a reduced work hardening makes the elongation value smaller. Thus, the observed values for tensile strength and elongation are in accordance with what could be expected. However, this is not the case for the creep tests. For the creep tests, a reduction in load carrying by 9% would give an increase in the strain rate by at least a factor of 200 with a typical creep stress exponent of 65 to 100 at 50 ºC. This is obviously much more than observed. The simplest explanation would be that the damaged zone is overestimated. Considering the comparatively short charging times of about 65 h, this could well be the case. It should also be noted that non-negligible creep rates were measured at very low stresses of 120 and 140 MPa in pure water, which is not consistent with studies in air on Cu-OFP.

At Swerea-KIMAB a few attempts have been made to reproduce the Finnish observations under nominally identical conditions. These attempts have failed. For example, no surface cracking has been found. Much lower creep strain rates have also been measured.

2.5 Modelling of electrochemical charging results

The electrochemical charging experiments described above gave two surprising results. First, a large number of hydrogen bubbles were formed. Although bubbles have been observed in the past, see section 2.3, their sizes were unexpectedly large in comparison to what previously had been found for electroless copper (Nakahara 1988). Second, hydrogen penetrated not much more than 50 μm into the material. Accurate measurements of the diffusion coefficient for hydrogen in copper are available also close to room temperature (Ishikawa and McLellan 1985). Available measurements of the diffusion coefficient have been analysed by Martinsson and Sandström (2012) and Magnusson and Frisk (2013a). If the measured diffusion coefficient is applied in the ordinary diffusion equation it would suggest a much deeper penetration of hydrogen than the one actually observed.

To understand the inflow of hydrogen a basic model has been developed. The most important change in the diffusion equation is that the inflow of hydrogen into the bubbles is taken into account. Already Wampler et al. (1976) suggested an expression for this inflow, and this expression has been used in the model. The resulting expression gives an inflow that is directly proportional to the number of bubbles per unit area and the diffusion coefficient, but independent of the bubble radius. It was observed that the bubbles primarily appear at grain boundaries, Fig. 1. In the model it is assumed that bubbles are nucleated at grain corners. From the expression for the inflow into the bubbles, the growth rate of the bubble radii can be derived. By comparing the shape of the bubbles close to the surface with elasto-plastic finite element modelling of bubbles with internal pressure, it was found that the internal pressure during the growth was about 400 MPa. The pressure could not be much lower because the bubbles would not grow and it could not be much higher because the shape of the bubbles at the surface would be different. In this way a partial differential equation for the diffusion of hydrogen and an ordinary differential equation for the growth of the bubbles have been set up (Martinsson and Sandström 2012).

The model is compared to experimental results in Fig. 2 to Fig. 5. In Fig. 2 the total amount of hydrogen gas (molecular hydrogen) as a function of distance from the surface is given. As can be seen the model values are well within the range of the observations. In Fig. 3 the variation of the bubble diameter as a function of depth into the material is shown. The size of the bubbles is reduced by about an order of magnitude when moving from the surface down to 50 μm into the material. Again each point in Fig. 3 (and in Fig. 4 and Fig. 5) is the average of about 20 measured bubbles.

PDF rendering: DokumentID 1420051, Version 1.0, Status Godkänt, Sekretessklass Öppen

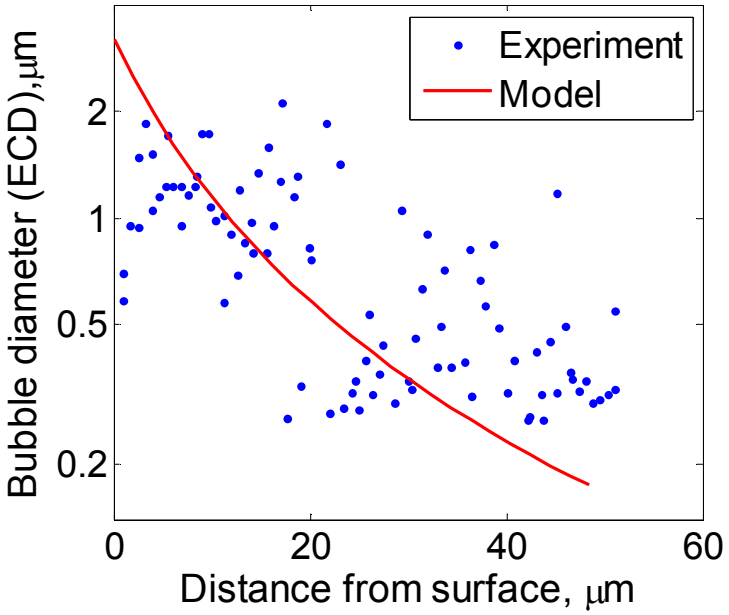

Fig. 3. Bubble diameter (equivalent circle diameter) as a function of distance from the surface after three weeks of charging (Martinsson and Sandström 2012).

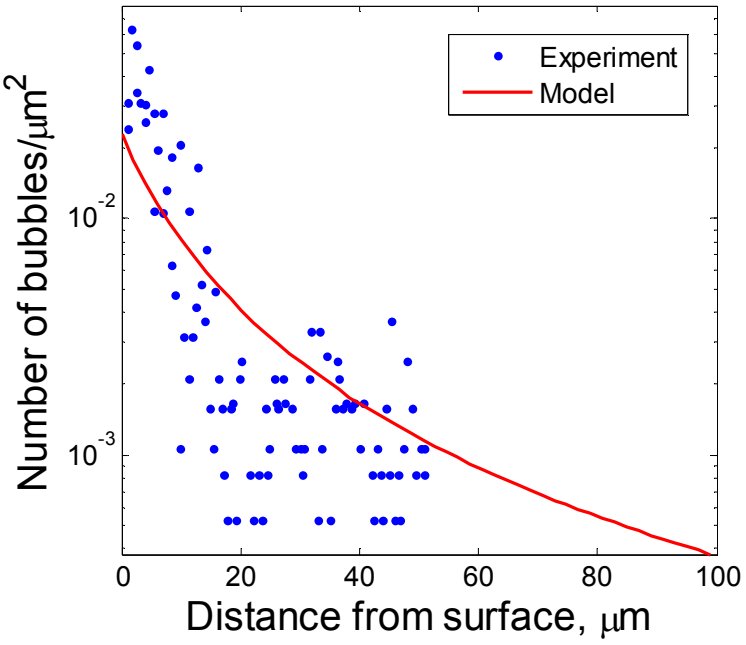

Fig. 4. Number of bubbles per unit area as a function of distance from the surface after three weeks of charging (Martinsson and Sandström 2012).

The number of bubbles per unit area is presented in Fig. 4. The reduction in this quantity when reaching a depth of 50 μm is a little more than a factor of 10. Since both the bubble diameter and the number of bubbles per unit area decrease as a function of distance from the surface, there is a rapid decrease in the area fraction of bubbles, Fig. 5. It is evident from Fig. 3 to Fig. 5 that the model can explain the observed size distribution of the hydrogen bubbles.

PDF rendering: DokumentID 1420051, Version 1.0, Status Godkänt, Sekretessklass Öppen

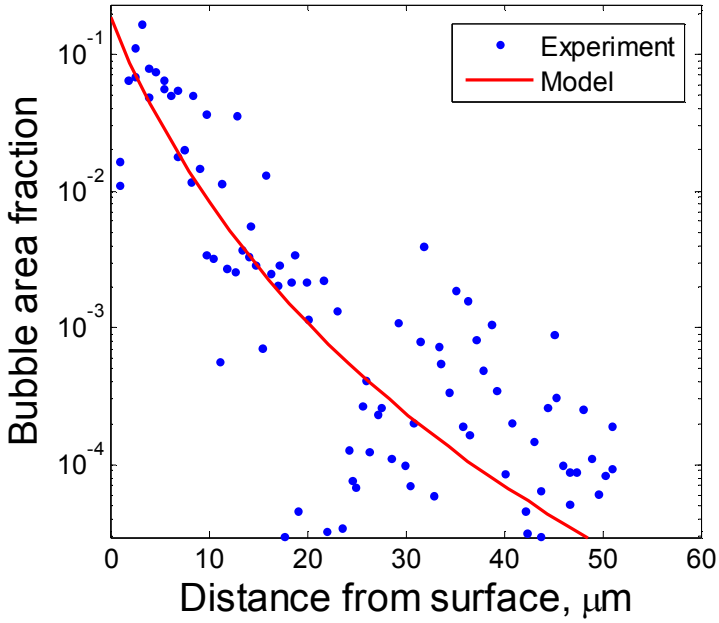

Fig. 5. Bubble area fraction as a function of distance from the surface after three weeks of charging (Martinsson and Sandström 2012).

3. Degassing

When leaving charged specimens at ambient conditions, it was discovered that the total hydrogen content was reduced (Martinsson et al. 2013). This degassing of hydrogen is important to understand. In the repository, hydrogen charging can only be expected during certain time periods. Charging will take place initially if water is present inside the insert and later if there is a leak in the copper shell. During an initial period of 300 years, gamma radiation is intense enough (<1 Gy/h) to cause radiolysis of the water, which results in the production of hydrogen gas and hydrogen containing reactive species (e.g. hydrogen peroxide).

To take degassing into account in the model, the outflow of hydrogen must be considered. At the surface of the bubbles the hydrogen molecules can dissociate into atomic hydrogen that can diffuse to the surface of the copper. This transport can be described with Sieverts' law. The outflow is proportional to the gas permeability of copper, the square root of the hydrogen pressure, and inversely proportional to the distance between the surface and the bubble (Sandström and Söderberg 2014). If this expression is introduced in the diffusion equation, a term of the same form is obtained, which is also proportional to the bubble radius. When the outflow of hydrogen takes place, the pressure in the bubbles is reduced. A separate equation for this pressure is also set up. The decrease in pressure is proportional to the same quantities as in the term for the outflow in the diffusion equation.

A system of three differential equations is obtained in this way that have to be solved simultaneously. The three independent variables are the hydrogen content in solid solution, the bubble radius, and the pressure (or density) in the bubbles. The hydrogen permeability plays an important role in these equations. Fortunately, recent measurements of the permeability close to room temperature exist (Horinouchi et al. 2013)

The use of the model where both charging and degassing is taken into account is illustrated for a case studied experimentally with charging for 500 h. At 500 h the charging was stopped

PDF rendering: DokumentID 1420051, Version 1.0, Status Godkänt, Sekretessklass Öppen

and then the specimen was left at ambient conditions. The (atomic) hydrogen content (in solid solution) as a function of time is shown in Fig. 6. After 5 h the hydrogen is more local to the surface than for situations at longer times. The bubbles are quite small initially and have less effect on the transport. A fast inflow would be observed if the role of the bubbles would be ignored. With small bubbles, the content is higher than at later times since the small bubbles allow less inflow. This can be seen after 20 h in Fig. 6. When the bubbles increase in size the inflow into them is raised and the matrix content is reduced, in particular well inside the material. The rate of change of the depth dependence is slowly reduced until the end of charging.

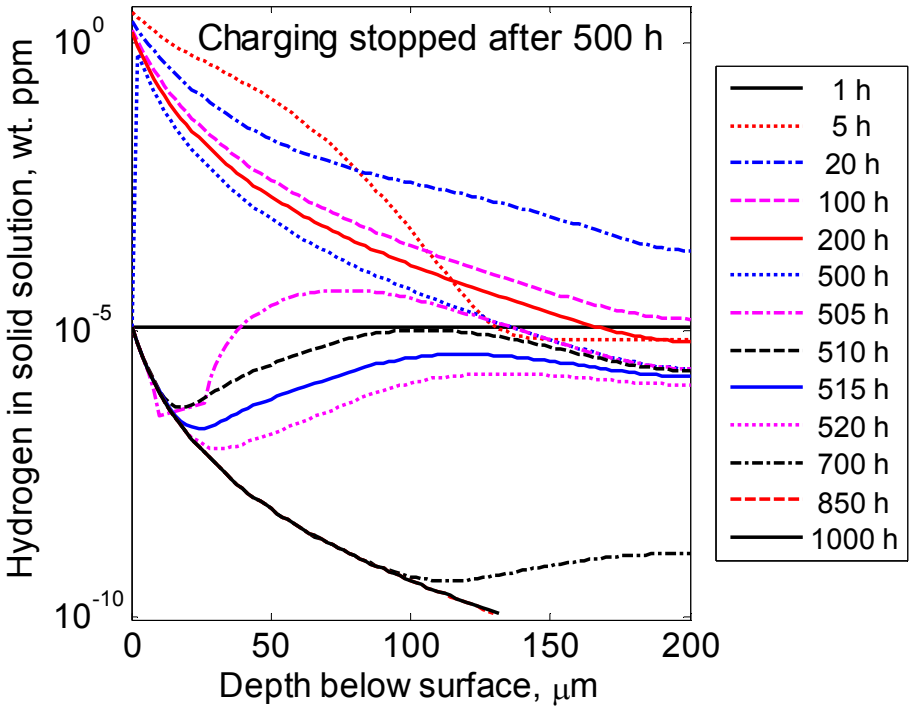

Fig. 6. Atomic hydrogen in solid solution versus depth below surface at different times. Charging was stopped after 500 h (Sandström and Söderberg 2014).

When the charging is stopped after 500 h, the distribution of hydrogen is dramatically changed. The content is reduced to the level of the atmospheric content of hydrogen ($1x10^{-7}$ kg/m^3 or $1.1x10^{-5}$ wt.ppm) within 5 h. The amount of hydrogen is then further reduced to very low levels inside the material. This rapid reduction is a result of the outflow from the surface. The outflow from the bubbles takes place at the same time but it is not large enough to compensate for the degassing from the surface.

The density of the hydrogen gas in the bubbles as a function time is illustrated in Fig. 7. The density remains constant as long as the charging takes place. When the charging is terminated, the outflow from the bubbles exceeds the inflow. The pressure in the bubbles drops. The origin of this effect is that the amount of hydrogen in solid solution drops to very low values, Fig. 6. The size of the bubbles remains constant. This is a direct consequence of the assumed plasticity model for the bubbles.

PDF rendering: DokumentID 1420051, Version 1.0, Status Godkänt, Sekretessklass Öppen

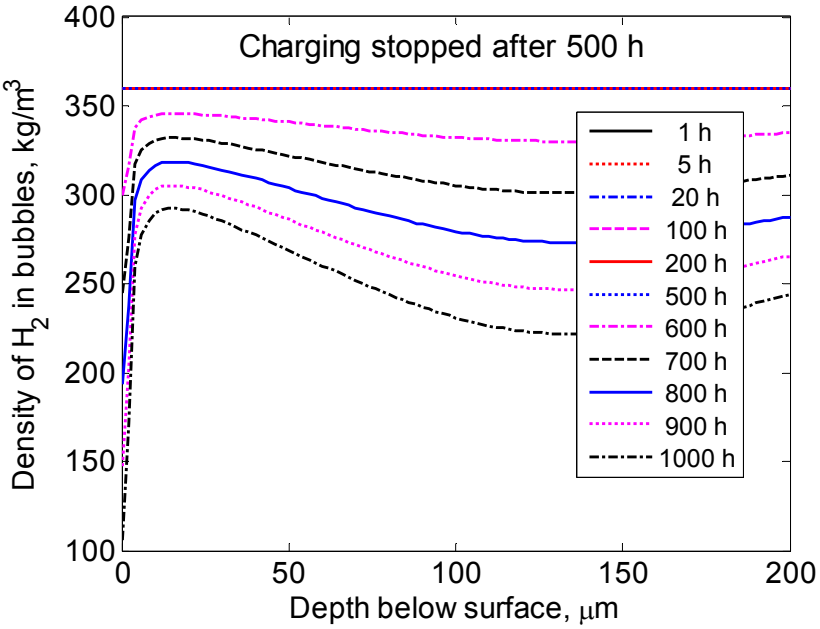

Fig. 7. Density of hydrogen gas in bubbles versus depth below surface at different times. The density is constant before the charging is stopped (Sandström and Söderberg 2014).

From the model, the total amount of hydrogen gas as a function of time can be computed. The result is shown in Fig. 8. During charging the amount of hydrogen is continuously increasing. When the charging is stopped the situation is reversed and there is a continuous drop in content. This drop is a direct consequence of the corresponding changes in the density in the bubbles, Fig. 7. The changes are largest at the surface and at intermediate depths of 125 to 150 μm.

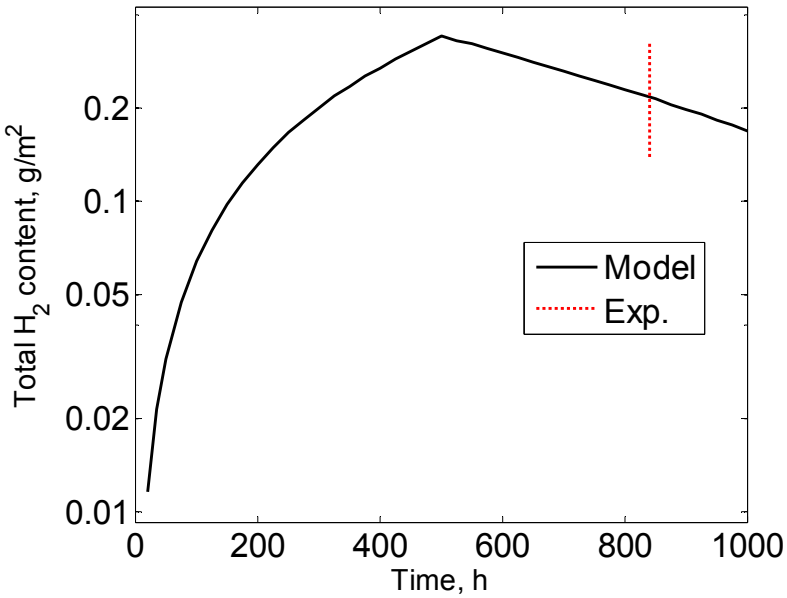

Fig. 8. Total molecular hydrogen content in the bubbles per unit surface area versus time. Model values are compared to the observations (Sandström and Söderberg 2014).

PDF rendering: DokumentID 1420051, Version 1.0, Status Godkänt, Sekretessklass Öppen

The observed amount of degassing after 2 weeks is shown in Fig. 8. It is in good agreement with the predictions. The error bar in the experimental results direct reflects the variation in the observations

4. Trapping of hydrogen

For a more complete understanding of degassing, it is important to know how the hydrogen is stored in copper. It is well known that hydrogen can be stored at defects and structural inhomogeneities such as dislocations, particles, inclusions, and grain boundaries. Such positions in the microstructure are often referred to as traps. The binding energies between the traps and hydrogen will control if they contribute to degassing. A fairly limited number of studies of hydrogen traps have been performed for copper (Wampler et al. 1976), whereas for nickel with identical lattice structure studies are available, see for example Oudriss et al. (2012). Also defects at the atomic level play an important role. In recent work, two types of traps at this level have been identified (Korzhavyi and Sandström 2014).

The binding energy of an H atom in the Cu lattice to a vacancy is calculated to be about 0.24 eV using ab-initio methods (Korzhavyi and Sandström 2014). This type of traps is quite shallow but can bind many hydrogen atoms since 6 hydrogen atoms can be associated to each vacancy. For an oxygen impurity in Cu, a vacancy is shown to be a deep trap which can in turn bind a hydrogen atom. This represents a deep trap for dissolved hydrogen with a binding energy of 1.23 eV. These energies apply to atomic hydrogen. The number of deep traps is proportional to the amount of oxygen in the material, since one hydrogen atom is bound to one oxygen atom.

Using modified McNabb and Foster equations (McNabb and Foster 1990), the amount of hydrogen locked to the two types of traps can be computed. If hydrogen and oxygen content are expressed in at.ppm, their relation is obvious. The maximum hydrogen and oxygen contents specified by SKB are 0.6 and 5 wt.ppm, respectively. This corresponds to 38 and 20 at. ppm, respectively, and these values have been used in the analysis.

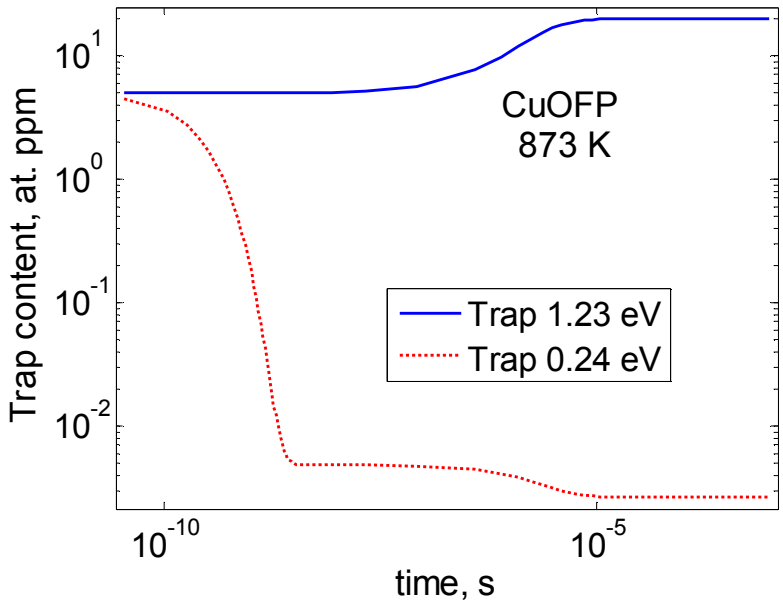

Fig. 9. Content of hydrogen in two traps with binding energies of 1.23 and 0.24 eV versus time at 873 K. Double logarithmic scale (Korzhavyi and Sandström 2014).

PDF rendering: DokumentID 1420051, Version 1.0, Status Godkänt, Sekretessklass Öppen

The variation of trap content with time for the two types of traps is illustrated in Fig. 9. The starting values are arbitrarily set to 5 at. ppm. The content of the deep trap is increased very rapidly at the expense of the shallow trap. The maximum content in the deep trap is close to 20 at. ppm, which is equal to the oxygen content. The temperature dependence of the stationary contents is illustrated in Fig. 10.

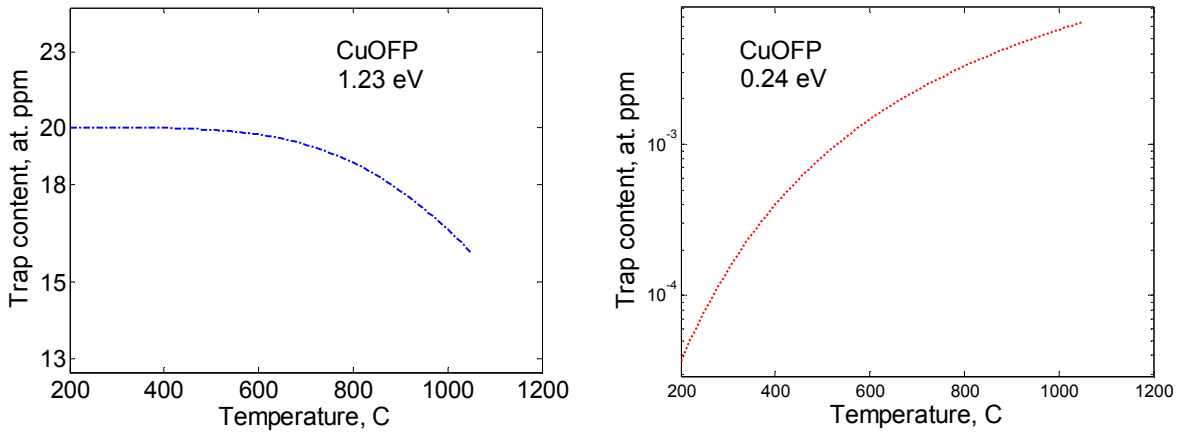

Fig. 10. Content of hydrogen in traps versus temperature; a) binding energy of 1.23 eV; b) binding energy of 0.24 eV (Korzhavyi and Sandström 2014).

The deep trap in Fig. 10 remains filled up to high temperatures. Only close to the melting point for copper, 1084 ºC, the content is reduced. The content in the shallow trap is low, but increases with temperature.

The fact that a deep trap is almost filled for temperatures up to the melting point has important technical implications. The hydrogen in the deep trap will be quite difficult to remove. This is in agreement with both experimental and industrial findings. To reduce the hydrogen content below 20 at. ppm, vacuum treatment of molten copper must be applied (Nagai and Sakai 1990). If there were no deep traps, the hydrogen could be degassed by simple heat treatment at high temperatures. Degassing in ultrahigh vacuum has been applied scientifically many times to analyse gas emission from copper. For example, Pope and Olson (1972) first treated copper specimens in vacuum at 250 ºC to eliminate all loosely bound hydrogen. Then the specimens were degassed in ultrahigh vacuum at 735-945 ºC to determine the outflow of hydrogen. This demonstrates again that high temperatures (and low pressures) are required to remove the firmly bound hydrogen.

5. Technical applications of the scientific results

Electrochemical charging of copper with hydrogen could possibly take place during a corrosion process. It has been demonstrated that electrochemical charging of copper gives rise to a thin layer with enhanced hydrogen content. In the tests this layer was found to be about 50 μm. The mechanical properties are believed to be affected only in this surface layer. Since the surface layer is only a minute fraction of the thickness of the copper shell, the mechanical integrity of the copper shell will not be affected even if the copper would be extensively charged. With the developed model it is possible to estimate the distribution of hydrogen after very long times of charging. In special cases the penetration depth could increase from 50 to 200 μm for large grain sizes, which is still far too small to influence the mechanical integrity (Martinsson et al. 2013).

PDF rendering: DokumentID 1420051, Version 1.0, Status Godkänt, Sekretessklass Öppen

If residual water is left inside the cast iron insert after the sealing of the canister, corrosion of the iron will take place and hydrogen will be generated. In addition, during an initial phase in the repository, some hydrogen charging of the copper canister material could take place due to gamma-radiolysis of the water, which creates hydrogen containing reactive species. On the outside of the copper shell the only hydrogen generating corrodant present is sulphide. However, due to the slow supply rate of sulphide, this is not expected to contribute significantly to hydrogen charging. The debated corrosion of copper in pure oxygen free water seems to be a very limited process (Bengtsson et al. 2013), which is likely to have a minor effect on the hydrogen charging.

The hydrogen inside the insert will diffuse into the iron and, for example be located at traps. In spheroidal graphite cast iron, which is the selected material for the insert, pearlite and graphite/ferrite interfaces represent strong traps for hydrogen, whereas graphite and ferrite are weaker traps (Takai et al. 2002). However, it is highly unlikely that the hydrogen will be further transported into the copper shell. This would represent thermal charging, which has been demonstrated to be slow or non-existing even at temperatures as high as 600 ºC.

PDF rendering: DokumentID 1420051, Version 1.0, Status Godkänt, Sekretessklass Öppen

References

Al-Marahleh G S, El-Amoush A S, 2005. Effect of cathodically charged hydrogen on the microhardness of pure copper. American Journal of Applied Sciences 2, 526–532.

Au M, 2007. High temperature electrochemical charging of hydrogen and its application in hydrogen embrittlement research. Materials Science and Engineering: A 454–455, 564–569.

Bengtsson A, Chukharkina A, Eriksson L, Hallbeck B, Hallbeck L, Johansson J, Johansson L, Pedersen K, 2013. Development of a method for the study of H_2 gas emission in sealed compartments containing canister copper immersed in O_2-free water. SKB TR-13-13, Svensk Kärnbränslehantering AB.

Butomo D G, Zedin N I, Mnushkin O S, 1968. Effect of oxygen on the susceptibility of copper to "hydrogen sickness". Metal Science and Heat Treatment 10, 184–185.

Caskey J G R , Dexter A H, Holzworth M L, Louthan J M R, Derrick R G, 1975. Hydrogen transport in copper. Materials Science Symposium of AIME.

Caskey G R, Dexter A H, Holzworth M L, Louthan M R, Derrick R G, 1976. Effect of oxygen on hydrogen transport in copper. Corrosion 32, 370–374.

Condon J B, Schober T, 1993. Hydrogen bubbles in metals. Journal of Nuclear Materials 207, 1–24.

Cotterill P, 1961. The hydrogen embrittlement of metals. Oxford: Pergamon. (Progress in Materials Science 9:4).

Horinouchi H, Shinohara M, Otsuka T, Hashizume K, Tanabe T, 2013. Determination of hydrogen diffusion and permeation coefficients in pure copper at near room temperature by means of tritium tracer techniques. Journal of Alloys and Compounds 580, Supplement 1, S73–S75.

Ishikawa T, McLellan R B, 1985. The diffusivity of hydrogen in copper at low temperatures. Journal of Physics and Chemistry of Solids 46, 445–447.

Kim J J, Byrne J G, 1985. Mechanical and kinetic effects of cathodic hydrogen charging of copper and of Cu–Al alloys. Materials Science and Engineering 74, 201–214.

Korzhavyi P A, Sandström R, 2014. Monovacancy in copper: trapping efficiency for hydrogen and oxygen impurities. Computational Materials Science 84, 122–128.

Louthan M R, 2008. Hydrogen embrittlement of metals: a primer for the failure analyst. Journal of Failure Analysis and Prevention 8, 289–307.

Louthan M R, Caskey G R, Donovan J A, Rawl D E, 1972. Hydrogen embrittlement of metals. Materials Science and Engineering 10, 357–368.

Lynch S, 2012. Hydrogen embrittlement phenomena and mechanisms. Corrosion Reviews 30, 105–123.

Magnusson H, Frisk K, 2013a. Self-diffusion and impurity diffusion of hydrogen, oxygen, sulphur and phosphorus in copper. SKB TR-13-24, Svensk Kärnbränslehantering AB. (In press.)

PDF rendering: DokumentID 1420051, Version 1.0, Status Godkänt, Sekretessklass Öppen

Magnusson H, Frisk K, 2013b. Thermodynamic evaluation of Cu-H-O-S-P system. Phase stabilities and solubilities for OFP-copper. SKB TR-13-11, Svensk Kärnbränslehantering AB.

Martinsson Å, Sandström R, 2012. Hydrogen depth profile in phosphorus-doped, oxygen-free copper after cathodic charging. Journal of Materials Science 47, 6768–6776.

Martinsson Å, Sandström R, Lilja C, 2013. Hydrogen in oxygen-free, phosphorus-doped copper: charging techniques, hydrogen contents and modelling of hydrogen diffusion and depth profile. SKB TR-13-09, Svensk Kärnbränslehantering AB.

McNabb A, Foster P K, 1990. New analysis of diffusion of hydrogen in iron and ferritic steel. Transactions of the Metallurgical Society of AIME 227, 618–627.

Nagai Y, Sakai S, 1990. Mass spectrometric observation of vacuum treated oxygen free copper. Vacuum 41, 2100–2102.

Nakahara S, 1988. Microscopic mechanism of the hydrogen effect on the ductility of electroless copper. Acta Metallurgica 36, 1669–1681.

Nakahara S, Okinaka Y, 1988. The hydrogen effect in copper. Materials Science and Engineering: A 101, 227–230.

Nakahara S, Okinaka Y, 1989. Defects induced in copper by cathodic charging of hydrogen. Journal of the Electrochemical Society 136, 1892–1895.

Nieh T G, Nix W D, 1980. The formation of water vapor bubbles in copper and their effect on intergranular creep fracture. Acta Metallurgica 28, 557–566.

Okinaka Y, Straschil H K, 1986. Effect of inclusions on the ductility of electroless copper deposits. Journal of the Electrochemical Society 133, 2608–2615.

Oudriss A, Creus J, Bouhattate J, Conforto E, Berziou C, Savall C, Feaugas X, 2012. Grain size and grain-boundary effects on diffusion and trapping of hydrogen in pure nickel. Acta Materialia 60, 6814–6828.

Panagopoulos C N, Zacharopoulos N, 1994. Cathodic hydrogen charging and mechanical properties of copper. Journal of Materials Science 29, 3843–3846.

Pope L E, Olson F A, 1972. Degassing of copper wires in an ultrahigh vacuum. II. Surface phenomena. Surface Science 32, 16–28.

Sandström R, Söderberg Å, 2014. Degassing of hydrogen after electrochemical charging of copper. (Submitted for publication.)

SKB, 2006. Kapsel för använt kärnbränsle. Konstruktionsförutsättningar. SKB R-06-02, Svensk Kärnbränslehantering AB. (In Swedish.)

Song J, Curtin W A, 2011. A nanoscale mechanism of hydrogen embrittlement in metals. Acta Materialia 59, 1557–1569.

Takai K, Chiba Y, Noguchi K, Nozue A, 2002. Visualization of the hydrogen desorption process from ferrite, pearlite, and graphite by secondary ion mass spectrometry, Metallurgical and Materials Transactions A 33, 2659–2665.

PDF rendering: DokumentID 1420051, Version 1.0, Status Godkänt, Sekretessklass Öppen

Wampler W R, Schober T, Lengeler B, 1976. Precipitation and trapping of hydrogen in copper. Philosophical Magazine 34, 129–141.

Yagodzinskyy Y, Malitckii E, Saukkonen T, Hänninen H, 2012. Hydrogen-enhanced creep and cracking of oxygen-free phosphorus-doped copper. Scripta Materialia 67, 931–934.

PDF rendering: DokumentID 1420051, Version 1.0, Status Godkänt, Sekretessklass Öppen